International Journal of Advanced Scientific Technologies , Engineering and Management Sciences (IJASTEMS-ISSN: 2454-356X) Volume.3,Special Issue.1,March.2017

AN EXPERIMENTAL POWER-LINES MODEL FOR DIGITAL ASICS BASED ON TRANSMISSION LINES

R. Priyadarsini[1] , C.H Kavya [2], A.Lasmika[3]
Academic consultant,
[1, 2,3]Department of ECE,
SPMVV,
TIRUPATHI, Andhra pradesh, India,
[1] *priyamtech.610@gmail.com*

ABSTRACT:We presented a transmission-line-based model developed to accurately describe the power and ground-line interconnections of modern digital ASICs. The proposed model employs transmission lines as the core component to properly describe both the capacitive and inductive behavior of the metal lines. In addition, the nonlinear frequency dependence of the line resistance, due to the skin-effect, is modeled with an additional lumped model. The model is completely derived from measurement data and allows describing both in-house and third-party ASICs. High-frequency -parameter measured data are used to benchmark the model. Finally, on-board voltage measurements of a Numonyx 64Mbit flash memory are performed and compared with transistor-level simulations.

I.INTRODUCTION

(content should font size 10 and time newroman)

Modern communication systems demand a continuous increase in bandwidth/data-rates and operating frequencies. In order to accomplish this goal, an increase in the level of parallelism of CMOS designs at the IC level is required (i.e., wide binary words and consequently wide bus structures). At the same time, the reduction of the propagation delay of a single output buffer induces a higher current during the transition. Thus, simultaneous switching of different output buffers will draw large currents in short time intervals (e.g., current pulses) from the I/O power lines (VDDQ/GNDQ), generating a large voltage surge/droop, which is referred to as power or ground bounce. To model interconnections, an RC network has been used . However, since inductance effects are neglected, this is a first-order approximation, and its accuracy decreases as frequency increases.

The output voltage waveforms in the presence of power bounce can be represented by a damped resonant waveform which is due to the power interplay between the inductor and the sum of the load and parasitic capacitor. Hence, it is crucial to include the inductive component in order to properly predict the power/ground bounce. While at the board and package level this is done by making use of 2-D and 3-D field solver programs, at the IC level, this is not done since most electronic design automation (EDA) programs cannot compute the inductive contribution of the complex structures of integrated power lines. To overcome this limitation, an *RLC* model was proposed [8], but the frequency-dependent transmission-line parameters are not taken into account in this model. Recently, solutions have been proposed to model the interconnections using transmission lines, nevertheless, these solutions required special test structures and particular for de-embedded techniques. The same problems are present with the general solution based on _-parameter model which is introduced in earlier.

We have used a different approach by using a transmission-line based model for the power lines, which allows a more accurate description of power-bounce phenomena in fast switching memories. The proposed method does not require any dedicated structure. Required structures are only used to extract parameters functional to the modeling process

The model extraction is based on experimental measurements and requires two additional pieces of information, namely the topology of each pad connected to the power line (e.g., an input/output buffer, clock pad, input buffer, or output buffer) and its relative position along the line (e.g., first, second etc.). Note that this information is known for both in-house and third-party devices.

This paper is organized as follows. First the transmission-line model including the memory core and the crosstalk model is described, and the extraction procedure for both in-house and third-party ASICs is illustrated. Then, the transmission-line-based model is evaluated, and its accuracy is determined for various layout topology configurations by means of electromagnetic (EM) simulations and measurement data (i.e., _-parameter measurements). Finally, signal integrity (SI) simulations are compared with accurate on-chip SI

measurements performed on a Numonyx flash memory, assessing the improved accuracy of the proposed model as compared with conventional RC models.

II. LITERATURE SURVEY

The transmission-line behavior can be described by dividing the VDDQ/GNDQ I/O power line into basic cells, each loaded with a capacitance representing the I/O buffer and some possible active and parasitic circuitry connected to the VDDQ/GNDQ line (Fig. 1). Therefore, each cell describes the power-line section connecting two consecutive capacitive loads. It is safe to assume that the parameters representing the lines will be the same for each basic cell, with the only exception being the lengt

The power-line section is represented as a transmission line whose characteristic impedance and electrical length are parameters to be extracted. In addition to the transmission line, an RLC subcircuit is introduced in order to include the frequency-dependent resistance due to the skin-effect. The aforementioned subcircuit consists of discrete elements and can be easily implemented in any Spice like simulator. The inductance L_{se} and resistance R_{se} of the skin-effect subcircuit are also model parameters to be extracted. Also note that other types of pads (i.e., clock pad, output buffer, or input buffer) might be connected to the VDDQ/GNDQ lines, providing a loading capacitance different from that associated with data pads. For this reason, the model uses a parameter to account for the different capacitance value associated with non-I/O

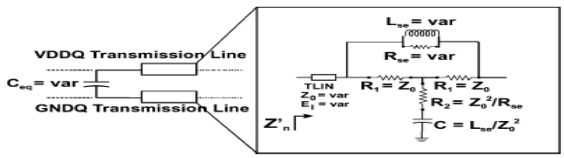

The complete model of the power line can be built by cascading the required number of basic cells, each constituted by a transmission-line element representing the line followed by the skin-effect sub-circuit.

III. PROPOSED METHOD

The discrete dipole approximation is a flexible technique for computing scattering and absorption by targets of arbitrary geometry. The formulation is based on integral form of Maxwell equations. The DDA is an approximation of the continuum target by a finite array of polarizable points. The points acquire dipole moments in response to the local electric field. The dipoles of course interact with one another via their electric fields, so the DDA is also sometimes referred to as the coupled dipole approximation. The resulting linear system of equations is commonly solved using conjugate gradient iterations. The discretization matrix has symmetries (the integral form of Maxwell equations has form of convolution) enabling Fast Fourier Transform to multiply matrix times vector during conjugate gradient iterations.

The method is a numerical computational method of solving linear partial differential equations which have been formulated as integral equations (i.e. in boundary integral form). It can be applied in many areas of engineering and science including fluid mechanics, acoustics, electromagnetics, fracture mechanics, and plasticity.

MoM has become more popular since the 1980s. Because it requires calculating only boundary values, rather than values throughout the space, it is significantly more efficient in terms of computational resources for problems with a small surface/volume ratio. Conceptually, it works by constructing a "mesh" over the modeled surface. However, for many problems, BEM are significantly less efficient than volume-discretization methods (finite element method, finite difference method, finite volume method). Boundary element formulations typically give rise to fully populated matrices. This means that the storage requirements and computational time will tend to grow according to the square of the problem size. By contrast, finite element matrices are typically banded (elements are only locally connected) and the storage requirements for the system matrices typically grow linearly with the problem size. Compression techniques (e.g. multipole expansions or adaptive cross approximation/hierarchical matrices) can be used to ameliorate these problems, though at the cost of added complexity and with a success-rate that depends heavily on the nature and geometry of the problem.

Mie solutions are implemented in a number of codes written in different computer languages such as Fortran, Matlab, Mathematica. These solutions are in terms of infinite series and include calculation of scattering phase function, extinction, scattering, and absorption efficiencies, and other parameters such as asymmetry parameter or radiation torque. Current usage of "Mie solution" indicate series approximation to solution of Maxwell's equations. There are several known objects which allow such a solution: spheres, concentric spheres, infinite cylinders, cluster of spheres and cluster of cylinders, there are also known series solutions for scattering on ellipsoidal particles.

BEM is applicable to problems for which Green's functions can be calculated. These usually involve fields in linear homogeneous media. This places considerable restrictions on the range and generality of problems suitable for boundary elements. Nonlinearities can be included in the formulation, although they generally introduce volume integrals which require the volume to be discretized before solution, removing an oft-cited advantage of BEM.

The Rayleigh scattering model breaks down when the particle size becomes larger than around 10% of the wavelength of the incident radiation. In the case of particles with dimensions greater than this, Mie's scattering model can be used to find the intensity of the scattered radiation. The intensity of Mie scattered radiation is given by the summation of an infinite series of terms rather than by a simple mathematical expression. It

can be shown, however, that Mie scattering differs from Rayleigh scattering in several respects; it is roughly independent of wavelength and it is larger in the forward direction than in the reverse direction. The greater the particle size, the more of the light is scattered in the forward direction.

The blue colour of the sky results from Rayleigh scattering, as the size of the gas particles in the atmosphere is much smaller than the wavelength of visible light. Rayleigh scattering is much greater for blue light than for other colours due to its shorter wavelength. As sunlight passes through the atmosphere, its blue component is Rayleigh scattered strongly by atmospheric gases but the longer wavelength (e.g. red/yellow) components are not. The sunlight arriving directly from the sun therefore appears to be slightly yellow while the light scattered through rest of the sky appears blue. During sunrises and sunsets, the Rayleigh scattering effect is much more noticeable due to the larger volume of air through which sunlight passes.

This is used to find approximate solution of partial differential equations (PDE) and integral equations. The solution approach is based either on eliminating the time derivatives completely (steady state problems), or rendering the PDE into an equivalent ordinary differential equation, which is then solved using standard techniques such as finite differences, etc.

In solving partial differential equations, the primary challenge is to create an equation which approximates the equation to be studied, but which is numerically stable, meaning that errors in the input data and intermediate calculations do not accumulate and destroy the meaning of the resulting output. There are many ways of doing this, with various advantages and disadvantages. The Finite Element Method is a good choice for solving partial differential equations over complex domains or when the desired precision varies over the entire domain.

4.3.3 Finite integration technique (FIT):

This is a spatial discretization scheme to numerically solve electromagnetic field problems in time and

The accuracy of the proposed approach was tested for an in-house Numonyx 64-Mb flash memory. First, using EM simulation of the VDDQ/GNDQ power lines, the proposed model accuracy is evaluated comparing simulated data with the extracted transmission-line model. For this comparison we used the layout of the memory, and performed EM simulations using the Momentum engine of Agilent's ADS simulator [ADS] to obtain the Y_{11} parameter of the line. This first extraction was done by assuming the simulation based on the Momentum data as the "measured" structure data.

Fig. 4 shows the magnitude and phase of the S_{11} parameter as obtained from the proposed model and the EM simulations. The plot shows a very good agreement in both magnitude and phase up to 2 GHz. In order to obtain a better agreement for higher frequencies, other models must be employed to account for the resistance modulation due to the skin-effect. Nevertheless, the tradeoff between the accuracy and the complexity of the model must be evaluated. The comparison is carried out with all of the buffers at logic high, while the model extraction procedure was performed with all of the buffers in the high-impedance condition, confirming that the model properly predicts the response of the power line under different buffer states.

The model was also compared with measured data. In this case, the measured data from the VNA was used as the reference data for the extraction of the parameters. Thus, by employing the procedure described above, the model parameters of the Numonyx memory are extracted using the high-impedance state (HZ) for the data buffer.

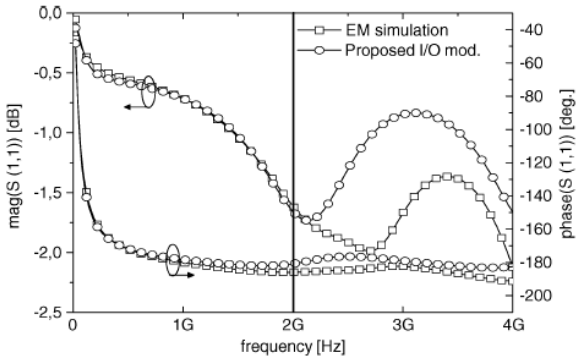

Fig. 4. Comparison of the S_1-parameter for the EM simulation and the proposed model when I/O buffers are all at logic high.

Fig. 5 shows a comparison between measured data and the proposed model for the output buffer in the logic-high state. The small disagreement at low frequency, highlighted by the black circle, can be explained by the low inductance value present on the bonded VDDQ pads, which provides little decoupling between the RF and the dc signal components.In contrast, the water droplets which make up clouds are of a comparable size to the wavelengths in visible light, and the scattering is described by Mie's model rather than that of Rayleigh. Here, all wavelengths of visible light are scattered approximately identically and the clouds therefore appear to be white or grey.

IV. PROPOSED ALGORITHM

Parameter extraction is an important part of model development. Many different extraction methods have been developed . The appropriate methodology depends on the model and on the way the model is used. A combination of a local optimization and the group device extraction strategy is adopted for parameter extraction.

Optimization strategy:

There are two main, different optimization strategies: global optimization and local optimization. Global optimization relies on the explicit use of a computer to find one set of model parameters which will best fit the available experimental (measured) data. This methodology may give the minimum average error between measured and simulated (calculated) data points, but it also treats each parameter as a "fitting" parameter. Physical parameters extracted in such a manner

might yield values that are not consistent with their physical intent

In local optimization, many parameters are extracted independently of one another. Parameters are extracted from device bias conditions which correspond to dominant physical mechanisms. Parameters which are extracted in this manner might not fit experimental data in all the bias conditions. Nonetheless, these extraction methodologies are developed specifically with respect to a given parameter's physical meaning. If properly executed, it should, overall, predict device performance quite well. Values extracted in this manner will now have some physical relevance.

Extraction Strategies:

Two different strategies are available for extracting parameters: the single device extraction strategy and group device extraction strategy. In single device extraction strategy, experimental data from a single device is used to extract a complete set of model parameters. This strategy will fit one device very well but will not fit other devices with different geometries. Furthermore, single device extraction strategy cannot guarantee that the extracted parameters are physical. If only one set of channel length and width is used, parameters related to channel length and channel width dependencies cannot be determined.

BSIM3v3 uses group device extraction strategy. This requires measured data from devices with different geometries. All devices are measured under the same bias conditions. The resulting fit might not be absolutely perfect for any single device but will be better for the group of devices under consideration.

Extraction Procedure:

These are six model parameters to extract (see Fig. 2): characteristic impedance Z_0, electrical length E_t of the single transmission line, resistance R_{sc} and inductance L_{sc} of the lumped subcircuit introduced to model the skin-effect, pad capacitance C_{eq} related to the single buffer, and scaling parameter K introduced to account for the different values of the I/O pad capacitances.

A two-port network can be represented by means of the Y –parameters

$$\begin{cases} I_1 = Y_{11}V_1 + Y_{12}V_2 \\ I_2 = Y_{21}V_1 + Y_{22}V_2. \end{cases} \quad (1)$$

The parameter extraction procedure is based on the comparison between the measured input admittance Y_{11} of the power line with the result obtained by the proposed model. The measurements are performed directly on the device pads, thus the measured data represent the power line without any parasitic component due to the bond-wires or the package. As shown below, the model yields an analytical equation for the input admittance which simplifies the extraction procedure. To calculate the Y_{11} parameter, we exploit the symmetry of the layout by assuming the physical and geometrical parameters for VDDQ and GNDQ lines to be equal (i.e., we assume the same characteristic.

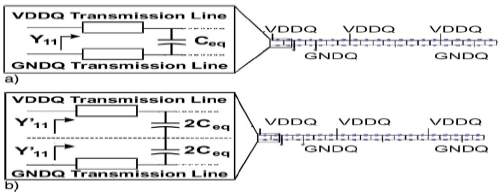

Fig. 3. Schematic representation of the circuit containing (a) VDDQ and GNDQ lines and (b) plane of symmetry between VDDQ and GNDQ line.

impedance and electrical length for each transmission-line element of VDDQ and GNDQ lines).We observe that Y_{11} at the input of the entire circuit is one half of the Y_{11}' seen at the input of the circuit obtained by considering only the VDDQ line with the buffer impedances divided by two (see Fig. 3). It is thus possible to calculate Y_{11}' using the model and then to obtain Y_{11}.

To calculate the input admittance, we make use of an iterative procedure. Denoting as $Z_{S,}$ the series impedance of the k_{th} cell, the impedance seen at the input of the $(k-1)_{th}$ cell can be calculated as

$$Z'_{k-1} = \left(Z'_k // Z_{Ceq}\right) + Z_{s,k-1}. \quad (2)$$

Using the above procedure, it is possible to express the input admittance in analytical form as a function of all model parameters.

$$Y_{11\_calc} = Y_{11}(Z_0, E_t, L_{sc}, R_{sc}, C_{eq}, k). \quad (3)$$

The model parameters are found by fitting the measured admittance Y_{11_meas} in the frequency domain. To this end, we define an error function f_{diff} as the distance between measured data and the model result as

$$f_{diff} = \frac{\sqrt{\sum_{i=1}^{N}(Y_{i11\_calc} - Y_{i11\_meas})^2}}{\sqrt{\sum_{i=1}^{N}(Y_{i11\_meas})^2}} \cdot 100 \quad (4)$$

where the sum is performed over the measured frequency values f_i, and Y_{11_rate} is given by (3). The model parameters are determined so as to minimize the error function f_{diff} over a specified frequency range. This extraction procedure was developed in the MATLAB environment using the *fmincon* function of the optimization toolbox. Physical considerations and a sensitivity analysis performed on the single parameters allow the definition of constraint conditions for all variables. Nevertheless, the *fmincon* function can lead to a local optimum solution, and this depends on the starting point chosen. Thus, in order to avoid a local minimum, we inserted this function in a nested "for" loop. defining different starting points (running along the constraint intervals). Although this is not the optimal solution, the global minimum is chosen as the minimum of the results.

Experimentally, S_{11} was measured up to 4 GHz by a VNA using coplanar high-frequency probes with the signal tip of the probe connected to VDDQ, and the ground tip connected to GNDQ. Since the comparison is made for the Y_{11} -parameter, a conversion from the S_{11}values (read on the VNA) to $Y_{11}$was made. Y-parameter data are measured only on a subset of output buffer configurations

and the parameter extraction is thus carried out by minimizing the function f_{diff} over these three different logic states.

TABLE I
EXTRACTED PARAMETERS FOR A THIRD-PARTY ASIC

Parameter	*Extracted Value*	*Err %*
Z_0	17.64 Ω	7.2
R_{se}	0.28 Ω	
L_{se}	0.118 nH	
E_t (1Ghz)	0.204°	
C_{eq} (HZ,FFFF,0000)	2.49 pF,2.66 pF,3.20 pF	
K	3.48	

The parameter E_t depends on the physical length of the power line section, and on the effective permittivity of the line. Two cases are considered.

1) If the layout of the power line is available, the physical lengths can be determined for all line sections connecting consecutive pads. In this case, the extraction procedure determines the unknown effective permittivity.

2) If the physical length is not available (as in the case of third-party devices), then a single "average" value for the physical length for all line sections is assumed in the extraction procedure.

This extraction procedure was applied to model the power line of a Numonyx flash memory. In this ,the physical lengths between two consecutive pads and loading capacitances related to I/O buffers and other pads were available . The length of the VDDQ/GNDQ lines is 4 mm. The minimum distance between two pads is 111 _m, and the maximum distance is 507 _m. The extraction procedure yielded a total error of 6.3%. On the other hand, assuming the same value for the physical length of the line sections , a slightly higher error of 7.2% is obtained. The different values of C_{eq} refer to the three different output buffer configurations.

Note that the small value of the transmission-line electrical length is to be attributed to the small memory size (i.e., 64 Mb). Larger and faster memory ICs will have larger power interconnect lines, hence justifying even more the use of distributed components for the modeling part.

V.SIMULATION RESULTS

To verify the model and accurately compare the simulations with the measurement results, transistor-level simulations are implemented in the Eldo Simulator from Mentor Graphics. Since the number of pads loading the VDDQ/GNDQ lines is 21 (16 I/O buffers and 5 non-I/O buffers), the lines are divided into 21 basic cells loaded by the complete netlist of the buffers. First, the extraction procedure described in the previous sections was performed to gather accurate model parameters. Then, the on0board microstrips and the connecting bond-wires were modeled to better include the measurement environment in the simulations. The modeling of the on-board microstrip was made by means of TDR analysis. The Lecroy digital sampling oscilloscope NRO9000 was used for this purpose. It is thus possible to model the on-board microstrip as a transmission-line component. All of the bonding wires are modeled by an RL subcircuit. Physical and geometric parameters of the bonding wire are used to describe it with a compact bond-wire model [17]. The RL subcircuit was obtained with a tuning of S-parameter response performed in the Agilent ADS environment. The S-parameter simulation was extended up to 2 GHz. The load of the buffers consists of the bonding wire, the microstrip on the board, and the load provided by the logic analyzer. The last contribution to the load of the buffers is related to the logic analyzer. To evaluate it again, a TDR response was used. Observing this response, one can recognize an inductive and then a capacitive behavior. It is thus possible to extract an LC subcircuit, by tuning the TDR response by means of Eldo simulations. The simulation was performed biasing the VDDQ line by an independent voltage source (to a value of 2 V) and switching simultaneously all DQ pads (the switching is defined inside the pad netlist but only for 16 of 21 pads). A second simulation was performed to compare the proposed model with a simple distributed RC model which is generally available for third-party ASICs. The basic cell of the power line is now represented by a single R loaded by the netlist of the buffer.

Fig. 8 compares the simulation results with the signal integrity measurement. Note the overshoot highlighted by the Eldo simulation using the proposed model and not present in the RC distributed model simulation. The high voltage drop shown by measured data most likely arise from the switching activity of the core, which is not yet fully incorporated in the model. The figure highlights a delay of the surge predicted by our model with respect to the measured data with a good agreement on the amplitude. This delay is lower than the delay present in the RC distributed model simulation.

In order to understand how this delay on the bounce influences the transition of the data, it is interesting to compare the simulated switching of a DQ pad with the measured data. Fig. 9 shows this comparison when a simultaneous switching of the 16 DQ buffers occurs RC and RLC models are compared with the proposed model.

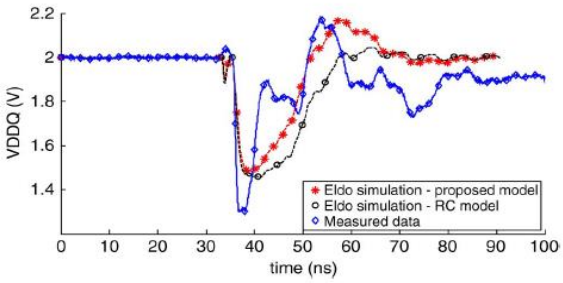

Fig. 8. Measurement point 3, comparison of the time-domain response between the measured data and Eldo simulations

The delay on the bounce predicted by the model is present also on the DQ data while the amplitude of the surge on the DQ signal is well predicted by the model. RLC model is better than RC for the period of oscillation point of view. In fact, it is very similar to the measured case. Nevertheless, the RLC model underestimates the ripple on the data and does not predict the correct rise time.

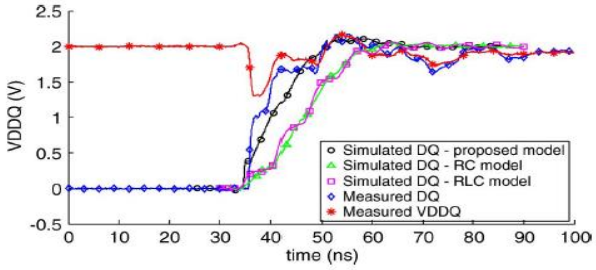

Fig. 9. Measured data and Eldo simulations of the switching of a DQ pad**.**

There are special purpose EDA tools that help the engineer perform all these steps on each signal in a design, pointing out problems or verifying the design is ready for manufacture. In selecting which tool is best for a particular task, one must consider characteristics of each such as capacity (how many nodes or elements), performance (simulation speed), accuracy (how good are the models), convergence (how good is the solver), capability (non-linear versus linear, frequency dependent versus frequency independent etc.), and ease of use.

An IC package or PCB designer removes signal integrity problems through these techniques:

Placing a solid reference plane adjacent to the signal traces to control crosstalk,Controlling the trace width spacing to the reference plane to create consistent trace impedance,Using terminations to control ringing,

Route traces perpendicular on adjacent layers to reduce crosstalk,Increasing spacing between traces to reduce crosstalk,Providing sufficient ground (and power) connections to limit ground bounce (this subdiscipline of signal integrity is sometimes called out separately as power integrity),Distributing power with solid plane layers to limit power supply noise.

Adding a preemphasis filter to the transmitter driving cell. See, for example,.[11]Adding an equalizer to the receiving cell[11]Improved clock and data recovery (CDR) circuitry with low jitter/phase noise[12]Each of these fixes may possibly cause other problems. This type of issue must be addressed as part of design flows and design closure.

VI CONCLUSION

In this paper, we described a novel distributed model based on transmission lines for the accurate description of power and ground lines in modern flash memory. The model can be extracted by means of experimental data. A new approach of on-die RF measurement to characterize and model digital ASIC power lines was utilized. The model was verified by means of EM simulations and on die measurements. Finally signal integrity simulations were performed to assess the accuracy of the model. In order to compare the model with signal integrity on die measurements, an extension of the model was made evaluating the on and off-die parasitics. Since there was good agreement between simulations and SI measurements, this model can be usefully employed to describe power- and ground-line interconnections of both in-house and third-party memories.

ACKNOWLEDGEMENT

We would like to thank Mrs.T.Sudha, Department of computer science SPMVV, and KMM Institute of Technology and Management [KMMITS].

REFERENCES

[1] Y. Yang *et al.*, "Design trade-offs for the last stage of an unregulated, long-channel CMOS off-chip driver with simultaneous switching noise and switching time considerations," *IEEE Trans. Comp., Packag., Manufact. Technol.*, vol. 19, no. 3, pp. 481–486, Aug. 1996.

[2] Y. S. Chang *et al.*, "Analysis of ground bounce in deep sub-micron circuits," in *Proc. IEEE VLSI Test Symp.*, 1997, p. 110.

[3] M. S. Haydt *et al.*, "Modeling the effect of ground bounce on noise margin," in *Proc. IEEE Int. Test Conf.*, 1994, pp. 279–285.

[4] A. Kabbani *et al.*, "Estimation of ground bounce effects on CMOS circuits," *IEEE Trans. Compon. Packag. Technol.*, vol. 22, no. 2, pp. 316–325, Jun. 1999.

[5] T. Sakurai, "Approximation of wiring delay in MOSFET LSI," *IEEE J. Solid-State Circuits*, vol. SC-18, no. 4, pp. 418–426, Aug. 1983.

[6] J. Rubinstein *et al.*, "Signal delay in *RC* tree networks," *IEEE Trans. Comput.-Aided Des. Integr. Syst.*, vol. CAD-2, no. 3, pp. 202–211, Jul. 1983.

[7] A. Deng *et al.*, "Generic linear *RC* delay modeling for digital CMOS circuits," *IEEE Trans. Comput.-Aided Des. Integr. Syst.*, vol. 9, no. 2, pp. 367–376, Apr. 1990.

[8] A. B. Kang *et al.*, "An analytical delay model for interconnects," *IEEE Trans. Computer-Aided Design*, vol. 16, pp. 1507–1514, Dec. 1997.

[9] Y. I. Ismail *et al.*, "Figures of merit to characterize the importance of on-chip inductance," *IEEE Trans. Very Large-Scale Integr. (VLSI) Syst.*, vol. 7, no. 4, pp. 442–449, Dec. 1999.

[10] R. Falah *et al.*, "Importance of on-chip inductance in designing *RLC* VLSI interconnects," in *Proc. Int. Conf. Microelectron.*, Dec. 2002, pp. 177–180.

[11] M. A. Mangan *et al.*, "De-embedding transmission line measurement for accurate modeling of IC designs," *IEEE Trans. Electron Devices*, vol. 53, no. 2, pp. 235–241, Feb. 2006.

[12] E. Yungseon *et al.*, "S-parameter-measurement-based high-speed signal transient characterization of VLSI interconnects on SiO2-Si substrate," *IEEE Trans. Adv. Packag.*, vol. 23, no. 3, pp. 470–479, Aug. 2000.

[13] "Analyse und modellierung der gesamtdaempfungsverluste von verlustbehafteten streifenleitungen," Darmstadt Univ. of Technol., Berlin,Germany, Oct. 1996.

[14] Idem Politecnico di Torino. Torino, Italy [Online]. Available: http:// www.emc.polito

[15] Y. Bard, *Non Linear Parameter Estimation*. New York: Academic, 1974.